A proposal of additions to the BM@N paper draft on p,d,t

Vadim Kolesnikov[a*]

[a]VBLHEP JINR, Dubna, Russia

[*]Corresponding author: Vadim, I., Kolesnikov; `kolesnik@jinr.ru`

1 Introduction

This draft describes results, obtained in the analysis of $p_t - y$ distributions of identified p, d, t from centrality selected Ar+A collisions collected by the BM@N experiment during 2016 and 2018 runs. Topics, which addressed in this document, include: 1) analysis of p_t-spectra and rapidity distributions of particles; 2) comparison of BM@N results for dn/dy and $\langle p_t \rangle$ with those from the STAR experiment (0-80% central Au+Au at 3 GeV); 3) study of baryon rapidity spectra and baryon rapidity loss in centrality selected Ar+A collisions; 4) study of the mass dependence of nuclear cluster yields. The content of Items 1-2 (Sections 2,3 of the current document) is not an alternative for the results from the paper draft and can be used as a cross-check. The results, presented in Sections 4,5 of this document (Items 3, 4) are new and suggested by us for further consideration by the BM@N collaboration.

2 Some analysis details

The data set, used in this analysis, includes 16.3M Ar+A collisions at center-of-mass energy $\sqrt{s_{NN}} = 3.1$ GeV. For each target specie, 0-40% central collisions were selected using information about charged track multiplicity in the detector. The number of participating nucleons for every beam-target combination was estimated with the DCM model (see Table 1).

First, fully corrected p_T-distributions of protons, deuterons, and tritons were obtained in rapidity intervals of $\Delta y = 0.2$. Systematic errors for particle yields in $(p_T - y)$ bins are quoted in Table 1 of the paper draft. These numbers were added in quadrature to statistical errors in every phase-space bin. As an example, resulting p_T-spectra for protons from 0-40% central Ar+Sn reactions are shown in Fig 1. The distributions are fitted to a function:

$$p_T e^{-(m_T - m)/T}, \tag{1}$$

where $m_T = \sqrt{p_T^2 + m^2}$, m – rest mass, and T is the slope parameter ('effective temperature'). The fit results are shown in the figure as solid curves and the slope parameter value is indicated in the legend. As one can see, the used single exponential form represents the proton spectra rather well, thus the fit function can be extrapolated into the unmeasured p_T-range to get the total integral of the distribution. The rapidity density dn/dy is obtained by adding the integral of the fit function over the uncovered p_T-regions to the sum of all data points. The extrapolation varies only slightly with the target atomic mass number and amounts from 5% to 30%, from 10% to 48%, and from 16% to 57% for protons, deuterons, and tritons, respectively. Figures 2 and 3 show p_T-spectra for deuterons and tritons for central Ar+Sn collisions.

A note: as one can see in Fig. 2, a single-exponential form does not describe p_T-spectra of deuterons near the beam rapidity ($y_{beam} = 2.16$). The low-p_T part of these spectra is much steeper than the high-p_T one. A guess (suspicion)

Table 1: DCM model predictions for the total number of participants N_{part}^{tot} and for the number of participants in the incoming Ar beam N_{part}^{proj} for 0-40% central and peripheral (centrality >40%) Ar+A collisions.

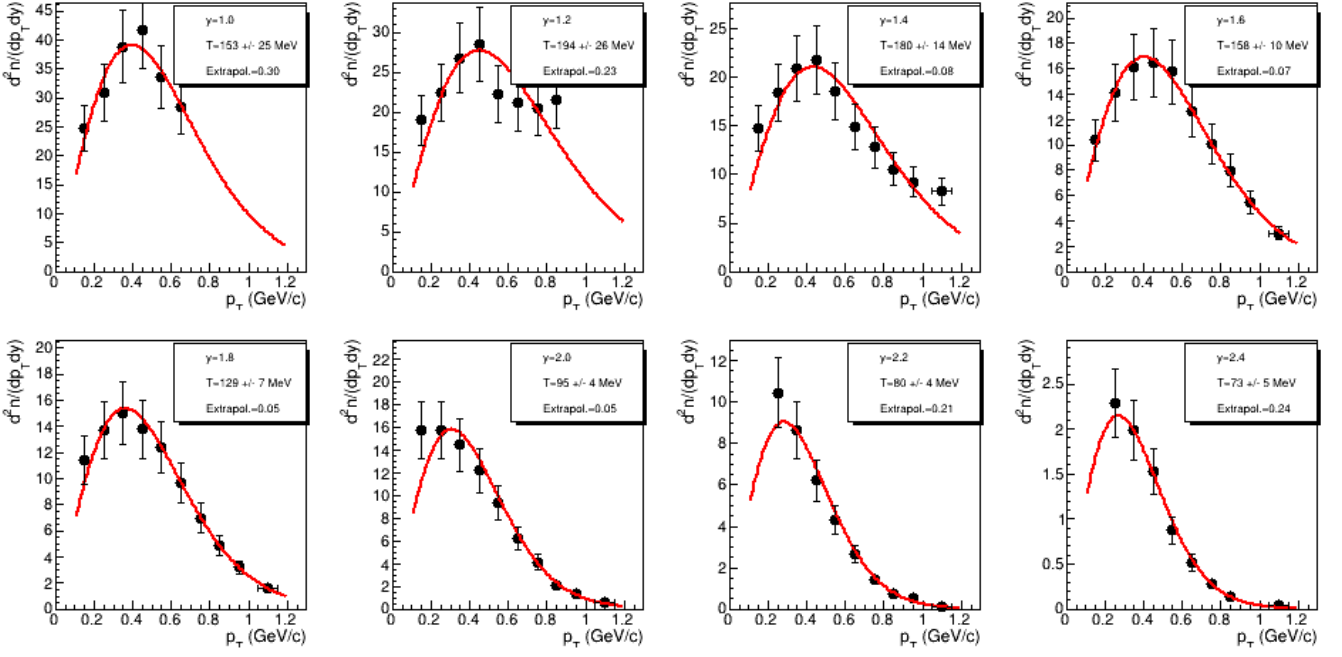|	Ar+C	Ar+Al	Ar+Cu	Ar+Sn	Ar+Pb
$N_{part}^{proj}(0-40\%)$	20.7	26	32	35	37
N_{part}^{tot} (0-40%)	30.0	45.5	77	116	169
N_{part}^{proj} (>40%)	5.6	6.9	9.4	11.7	14.7
N_{part}^{tot} (>40%)	9.1	13.0	21.6	31.1	47.3

Figure 1: p_T-spectra of protons from central Ar+Sn collisions in rapidity slices. The fit function is shown by the line, the value of the slope parameter and the estimate for the fraction of the extrapolation to the unmeasured region in the dn/dy value are indicated.
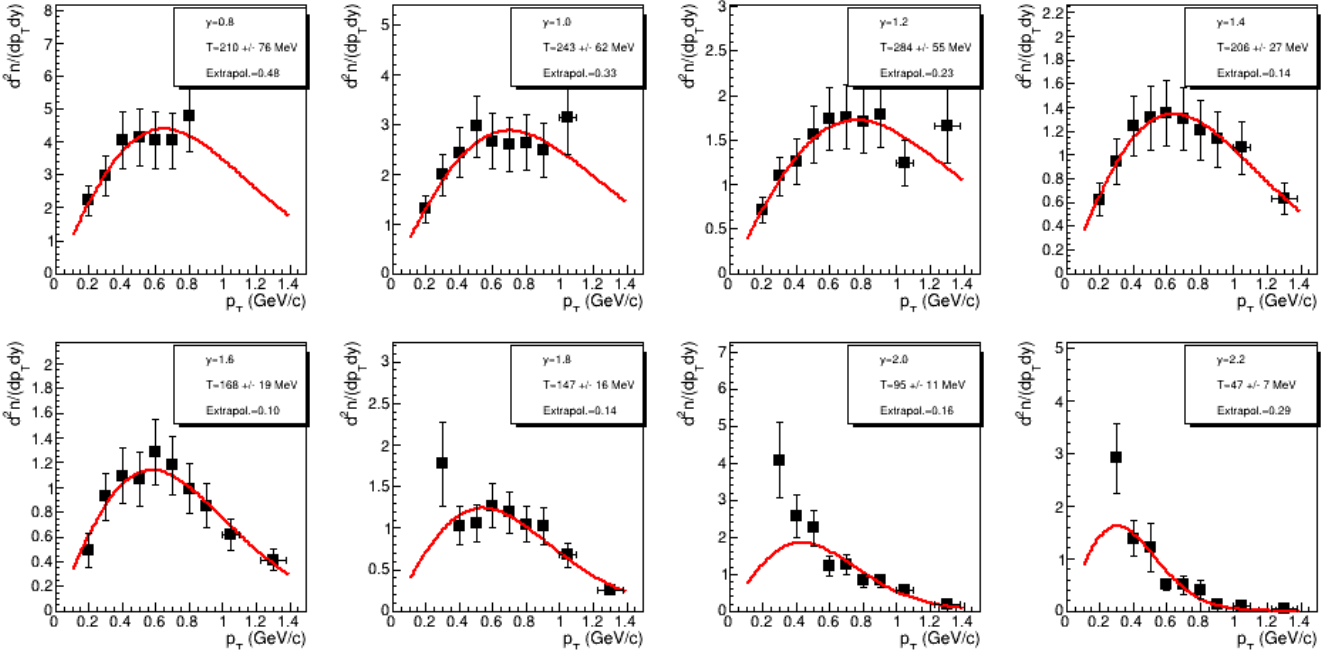

Figure 2: p_T-spectra of protons from central Ar+Sn collisions in rapidity slices. The fit function is shown by the line, the value of the slope parameter and the estimate for the fraction of the extrapolation to the unmeasured region in the dn/dy value are indicated.
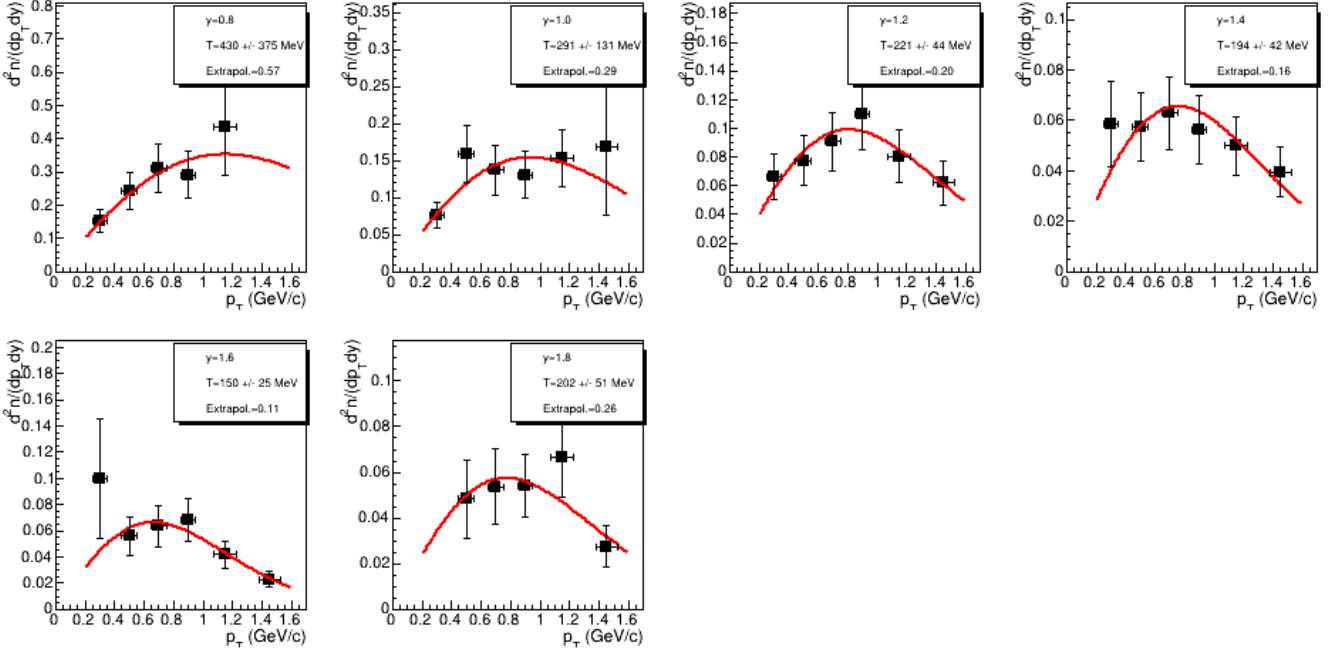
Figure 3: p_T-spectra of tritons from central Ar+Sn collisions in rapidity slices. The fit function is shown by the line, the value of the slope parameter and the estimate for the fraction of the extrapolation to the unmeasured region in the dn/dy value are indicated.

is that the contribution of fragmented ^4He nuclei (see Fig.4 in the paper draft) was not correctly estimated. The dn/dy value for deuterons in these bins was taken equal to the integral of the fit function, and the difference between the two estimates for the rapidity density (one from the fit function and another from the sum of data points) is added to the error in dn/dy.

3   Comparison of BM@N measurements with STAR data

Recently, the STAR experiment at RHIC has published results from the fixed target program [5]. Spectra and yields of $p, d, t, ^3He$ are measured in several centrality bins in Au+Au collisions at $\sqrt{s_{NN}} = 3$ GeV. Although the geometry and longitudinal distributions of produced particles in asymmetric Ar+A collisions differ from those in gold-gold interactions, it is expected that the yields near midrapidity can be directly compared for systems of similar volume (characterize by the number of participants N_{part}). In Fig. 4 (left panel), we present rapidity distributions of p, d, t from Ar+Al (0-40%, $N_{part}^{proj} = 26$) and Au+Au (40-80%, $N_{part}^{proj} = 20$). BM@N data are drawn by solid symbols, the results from the STAR experiment (scaled by the ratio of the numbers of participants in projectiles) are plotted by open ones. As one see, particle rapidity densities from Au+Au and Ar+Al collisions, indeed, agree at midrapidity (the difference between experiments does not exceed 20% at $y = 0$).
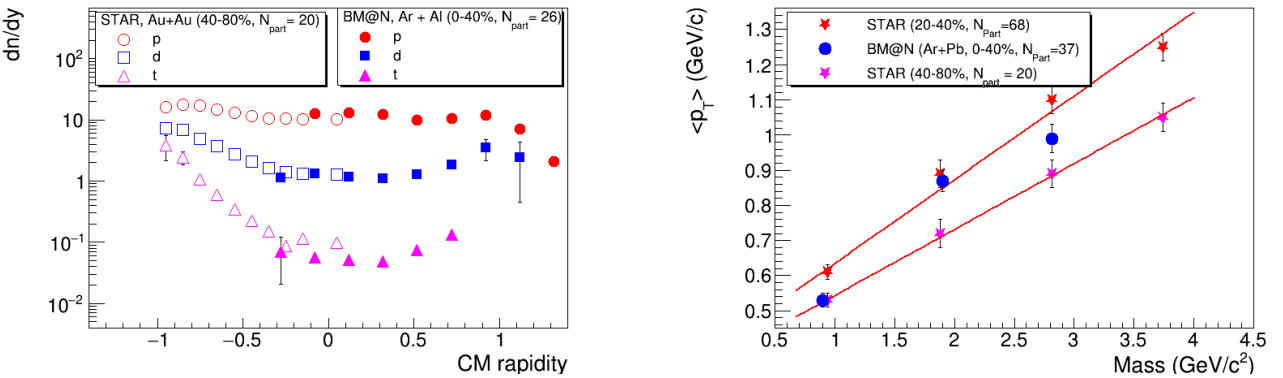

Figure 4: Left: Rapidity density dn/dy for p, d, t from 0-40% central Ar+Al collisions (solid symbols) and 40-80% Au+Au collisions (open symbols). STAR data are from [5]. Right: $\langle p_T \rangle$ of $p, d, t, ^3He$ in Au+Au (stars) and Ar+Pb (circles) collisions. STAR data are from [5], linear fits to STAR data points provide a guidance on the trend.

Mean transverse momentum $\langle p_T \rangle$ of particles was determined in the rapidity range $0.2 < y < 0.4$ GeV/c, where the BM@N has the largest p_T coverage. In Fig. 4 (right panel), $\langle p_T \rangle$ for p, d, t from 0-40% Ar+Pb collisions ($N_{part}^{proj} = 37$)

are shown together with STAR data for 20-40% ($N_{part}^{proj} = 20$) and 40-80%($N_{part}^{proj} = 68$) Au+Au collisions. Mean transverse momentum increases with particle mass, the observed increasing trend is different in Au+Au and Ar+Pb collisions: linear trend for the STAR data (steeper in more central collisions) and convex-like dependence for the BM@N measurements. The observed difference can be traced back to the fact that although the particle yields are approximately scale with the number of participants, the radial collective velocity profiles and the freeze-out nucleon density, which define the mass dependence for $\langle p_T \rangle$, can be different in central Ar+Pb and semi-central Au+Au interactions.

4 Baryon rapidity distributions, stopping and rapidity loss in Ar+A

The incoming nucleon loses its momentum during the collision and the mechanism of baryon transfer over finite rapidity distances (baryon stopping [1]) is an important theoretical problem for many years [2]-[4]. The baryon density, attained in high energy nuclear collisions, is a crucial quantity governing the reaction dynamics and the overall system evolution, including eventual phase transformations in dense nuclear matter. The measurement of rapidity distributions of stopped baryons in heavy ion collisions for different combinations of projectile and target as well as at different impact parameters provides essential constrains for the possible dynamical scenarios of baryon charge transfer. The advantage of the BM@N experiment at NICA is that the experimental arrangement of the detector makes it possible to measure the distribution of protons and light nuclei (d, t) over a rapidity interval [1.0 - 2.2]. This rapidity range is wide enough to include particle rapidity density not only near the midrapidity ($y_{CM} = 1.08$), but also at the rapidity of the incoming nucleus, in contrast to the situation at the collider, where the acceptance of collider experiments does not include this range. Together with a sufficient p_T-coverage for nuclear clusters in BM@N, it makes possible to better determine the shape of the rapidity density distribution and derive information about rapidity and energy loss in the reaction.

The total baryon number in Ar+A collisions at NICA/BM@N energies is basically determined by nucleons and light nuclei ($d, t, ^3$He). To obtain the baryon rapidity distribution, we add up the yield of protons, deuterons and tritons in every rapidity bin multiplied by the number of nucleons in compound particles. The obtained distribution should then be corrected for the fraction of unmeasured baryons: neutrons, hyperons and ^{3}He nuclei. Calculations with the PHQMD model indicate the n/p-ratio of about 1.1 in the forward hemisphere for all reactions. We assume that the $t/^3$He ratio is equal to n/p. The total number of baryons B in a rapidity bin was then calculated as

$$B = 2.1 \cdot p + 2.0 \cdot d + 5.7 \cdot t$$

Hyperons contribute less than 2% to the baryons and were not accounted for. Resulting baryon rapidity distributions for Ar+Cu collisions are shown in Fig. 5: the left panel shows the results for 0-40% central collisions, and the right one is for peripheral collisions. As one can see, more baryons are transported to midrapidity in the more central collisions leading to a dramatic difference in the shapes of dn/dy distributions. To describe those shapes, we fitted the measurements to a 3rd order polynomial in y^2; the fit results are shown in Fig. 5 by solid curves. Integrating rapidity distributions over the forward rapidity range $(0 - y_{beam})$, one can get an estimate for the number of participating nucleons in the projectile nucleus N_{part}^{proj}. The results of the integration are shown in the panel's legends, the quoted error for N_{part} are the errors of the sum of experimental points within the same rapidity range. While in peripheral A+A collisions the projectile and target regions in the baryon rapidity distributions are well separated from each other, those are broadened and may start to overlap in central collisions. The situation may become even worse in strongly asymmetric collisions, like Ar+Pb, where projectile and target baryons can mix strongly in the forward rapidity region. To clarify the issue, we got a guidance from the DCM model, which simulated Ar+A collisions of the defined centrality. The number of participating nucleons in these events are counted in the projectile and target nucleus separately. The model predictions for the number of projectile participants are shown in the legend of Fig. 5. As one can see, for central collisions the agreement between the total number of baryons from data points and the number given by the model is satisfactory. From that one can conclude that the overlap of target and projectile baryons is not enough to affect strongly the shape of rapidity distribution and to result in an additional uncertainty in the determination of N_{part} and rapidity loss values.

The mean rapidity loss is calculated as

$$\langle \delta y \rangle = y_b - \langle y \rangle, \tag{2}$$

where y_b is the rapidity of the projectile before the collisions and

$$\langle y \rangle = \frac{\int_0^{y_b} y \frac{dn}{dy} dy}{\int_0^{y_b} \frac{dn}{dy} dy} \tag{3}$$

Usually, it refers to net-baryons, i.e. baryons minus antibaryons. At NICA/BM@ energies, however, the production of antibaryons is so small that the difference between baryons and net-baryons is negligible. The mean rapidity was calculated from the integral of the fit function to the baryon rapidity distribution over the range $(0 - y_{beam})$, the final results for $\langle \delta y \rangle$ are listed in Table 2. As one can see, $\langle \delta y \rangle$ in central Ar+A collisions is higher than that in peripheral collisions, the excess (central collisions over peripheral) is of about 10% and 30% in Ar+C and Ar+Pb, respectively.
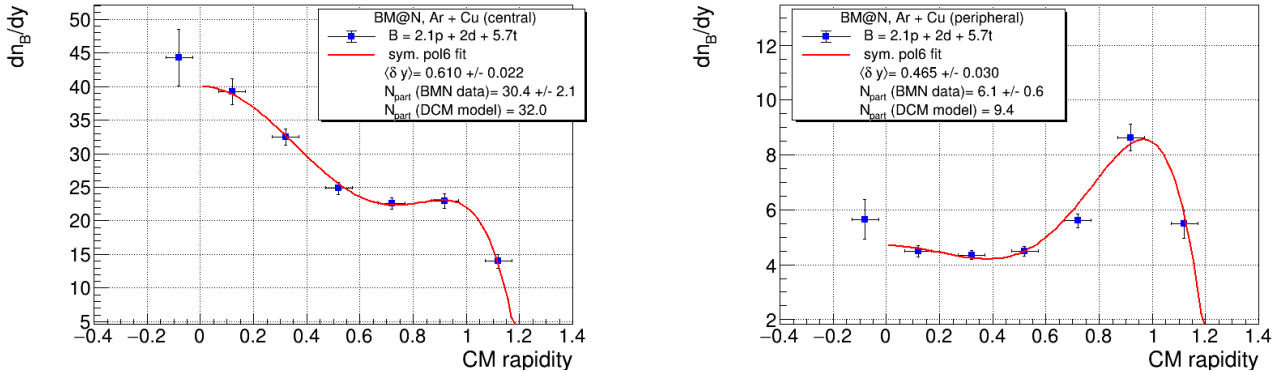
Figure 5: Left: Rapidity distribution of baryons in 0-40% central Ar+Cu collisions. The measurements are shown by symbols, a fit to a 3rd order polynomial in y^2 is drawn by the curve. Estimates for the number of participants in the projectile and for the mean rapidity loss $\langle \delta y \rangle$ are shown in the legend. Right: same for peripheral Ar+Cu collisions.

Table 2: Mean rapidity losses $\langle \delta y \rangle$ in Ar+A reactions.

	Ar+C	Ar+Al	Ar+Cu	Ar+Sn	Ar+Pb
0-40%	0.44 ± 0.04	0.54 ± 0.02	0.61 ± 0.02	0.65 ± 0.03	0.67 ±0.03
>40%	0.40 ± 0.02	0.44 ± 0.03	0.47 ± 0.03	0.50 ± 0.02	0.52 ± 0.02

BM@N results on rapidity loss can be compared to those from the STAR experiment [5]. Comparison of collision systems with different geometry and size parameters can be done using variable $X_{part} = N_{part}^{proj}/A_{proj}$, where N_{part}^{proj} is the number of participants in the projectile and A_{proj} is the mass number of the projectile (potential maximum number of participating nucleons in the projectile). X_{part} is larger in more central collisions and rises with increasing the target mass number for the fixed centrality. Moreover, using this variable allow us to put asymmetric and symmetric nucleus-nucleus collisions on a similar footing.

A compilation of rapidity loss values from Ar+A and Au+Au collisions is presented in Fig. 6. BM@N results for central and peripheral collisions are drawn by solid and open circles, respectively. STAR measurements in several centrality intervals (0-10%, 10-20%, 20-40%, and 40-80%) are plotted by stars. The X_{part} values are calculated using the DCM model predictions for the number of participating nucleons in the projectile tabulated in Table 1. The observed trend for the mean rapidity loss is apparent from the figure: $\langle \delta y \rangle$ rises with the collision centrality and the target mass. It is interesting to note that $\langle \delta y \rangle$ in 0-40% central Ar+Pb collisions is larger than that in 0-10% central Au+Au interactions. A possible explanation of this observation is the following. In central collisions of asymmetric nuclei, every participating nucleon in the (smaller in size) projectile can "see" the full diameter of the target nucleus, thus, interacting several times and slowing down more effectively. In contrast, even in central collisions of heavy nuclei of an equal size, a sizeable fraction of participating projectile baryons interact with a few target baryons and therefore do not contribute much to the stopping.

The energy dependence of nuclear stopping power is presented in Fig. 7 (left panel). Experimental data from AGS [6], SPS [7], and RHIC [8, 5] experiments are drawn with symbols of corresponding colors. Heavy-ion collisions are shown by solid symbols, $p + p$ data from AGS are depicted by open ones. We did not find any experimental data on stopping in $p + p$ collisions at NICA energies, but, assuming that for a given beam energy $\langle \delta y \rangle$ in peripheral A+A collisions agrees with the corresponding $p + p$ value, we present $\langle \delta y \rangle$ for peripheral Ar+C from BM@N as a $p + p$ proxy in the NICA energy range (see open purple circle in the figure). As one can see, the rapidity loss shows an increase with energy changing the slope of the increase above the top SPS energy. In contrast, the relative rapidity loss $\langle \delta y \rangle/y_{beam}$ saturates from NICA to SPS energies (see Fig. 7, right panel), and then decreases with energy indicating an increase in the nuclear matter transparency at RHIC energies. Data indicate also that the mean rapidity loss from $p + p$ collisions and peripheral Ar+C interactions do not scale with y_{beam}.

5 Study of the mass dependence of particle yields

It has been established experimentally that cluster production yields decrease exponentially with the atomic mass number A [9, 10]. As an example, Fig. 8 (left panel) presents midrapidity dn/dy for $p, d.t$ as a function of A from

Table 3: Mean rapidity losses $\langle \delta y \rangle$ in Au+Au collisions from the STAR experiment [5].

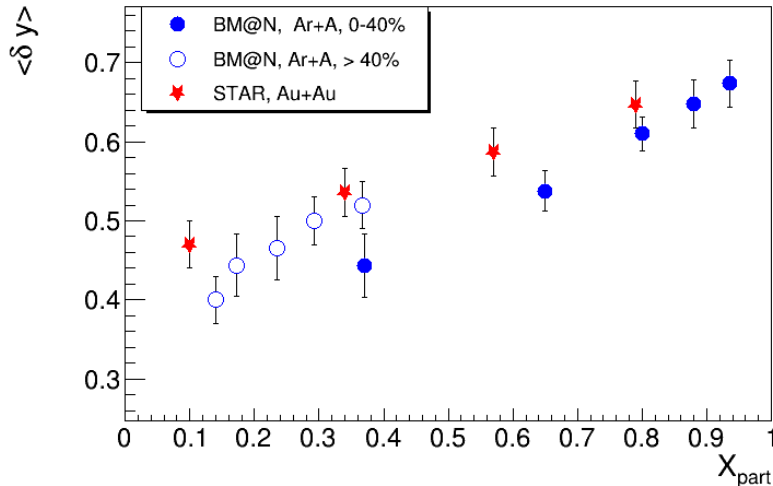| 0-10%	10-20%	20-40%	40-80%
0.65 ± 0.03	0.59 ± 0.03	0.54 ± 0.03	0.47 ± 0.03

Figure 6: Mean rapidity loss $\langle \delta y \rangle$ in Ar+A (BM@N experiment, this study) and Au+Au collisions (STAR experiment [5])
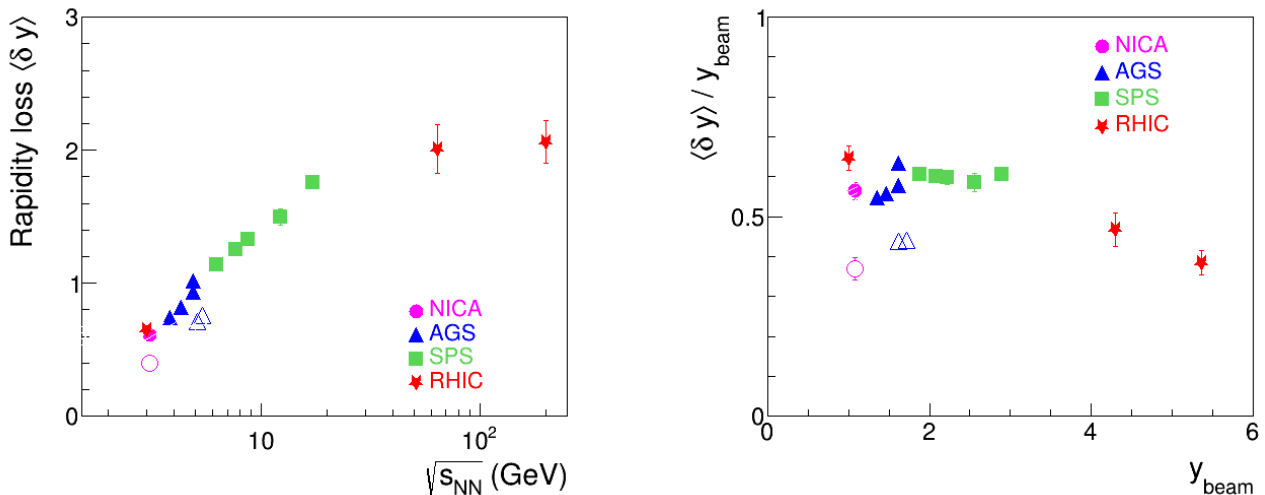
.

Figure 7: Left: An excitation function of mean rapidity loss in A+A collisions. $p+p$ data from AGS [6] and peripheral Ar+C collisions (this study) are shown by open symbols. Right: Mean rapidity loss divided by y_{beam}.

0-40% central Ar+Sn collisions. The A-dependence of yields was fitted to a form:

$$dn/dy(A) = const/p^{A-1}, \tag{4}$$

where parameter p ('penalty factor') determines the penalty of adding one extra nucleon to a system.

The penalty factor is sensitive to the nucleon density attained in the reaction (the larger density the smaller penalty) and in the framework of a statistical approach it is determined as follows

$$p = e^{(m-\mu_B)/T}, \tag{5}$$

where μ_B, T, and m being the baryochemical potential, freezeout temperature, and nucleon mass, respectively.

The p-factors from central Ar+A collisions are shown in Fig. 8 (right panel) as a function of the midrapidity baryon density and listed in Table 4. One can see a small variation of p in central Ar+A collisions at NICA energies.

A standard method for the determination of the freeze-out parameters of the source (i.e. T and μ_B) is based on the analysis of hadron abundances in the framework of a thermal statistical model. An alternative approach is the use of Eq. 5. As reported in Ref. [11], the values of kinetic and chemical freeze-out temperatures are similar in heavy-ion collisions below $\sqrt{s_{NN}} = 5$ GeV. Thus, we can use the value of T obtained in the analysis of transverse spectra of particles and reported in the paper draft as a good estimate for the freeze-out temperature. Transforming Eq. 5, a formula for μ_B can be written as

$$\mu_B = m - T \ln p \tag{6}$$

The resulting (T, μ_B) freeze-out parameters for central Ar+A collisions are tabulated in Table 4 and shown in Fig. 9. Surprisingly, preliminary BM@N results follow the trend defined by world data and by the parameterization from Ref. [12] (drawn by the dashed line).
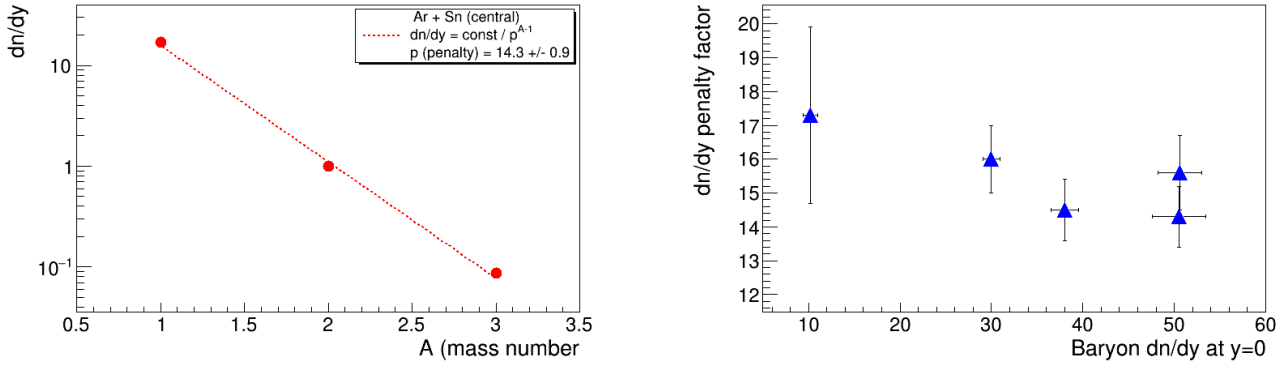
Figure 8: Left: Midrapidity $\mathrm{d}n/\mathrm{d}y$ for p, d, t from central Ar+Sn collisions. The dashed line is a fit to Eq. 4. Right: Penalty factor from central Ar+A collisions versus baryon rapidity density at $y = 0$.

Table 4: Penalty factor p, temperature T, and baryochemical potential μ_B in 0-40% central Ar+A collisions.

	p	T (MeV)	μ_B(MeV)
Ar+C	17.3 ± 2.6	89 ± 3	684 ± 40
Ar+Al	16.0 ± 1.0	76 ± 8	727 ± 30
Ar+Cu	14.5 ± 0.9	80 ± 5	724 ± 32
Ar+Sn	14.3 ± 0.9	74 ± 9	741 ± 34
Ar+Pb	15.6 ± 1.1	80 ± 10	718 ± 40

References

[1] W. Busza and A. S. Goldhaber, Phys. Lett. 139B, 235 (1984).

[2] G.C. Rossi and G. Veneziano, Phys. Rep. 63 (1980) 153.

[3] A. Capella and B. Z. Kopeliovich, Phys. Lett. B 381, 325 (1996)

[4] D. Kharzeev, Phys. Lett. B 378, 238 (1996)

[5] The STAR Collaboration, arXiv:2311.11020v1 [nucl-ex].

[6] F. Videbæk and O. Hansen, Phys. Rev. C 52 (1995) 2684.

[7] C. Blume, for the NA49 Collaboration, J. Phys. G 34 (2007) S951.

[8] Arsene I. et al (BRAHMS Collaboration) 2009 Phys. Lett. B 677 267.

[9] T.A. Armstrong et al (E864 Collaboration) Phys. Rev. C 61,064908 (2000).

[10] T. Anticic et al (NA49 Collaboration) Phys. Rev. C 94,044906 (2016).

[11] The STAR Collaboration, Phys. Rev. C 96,044904 (2017).

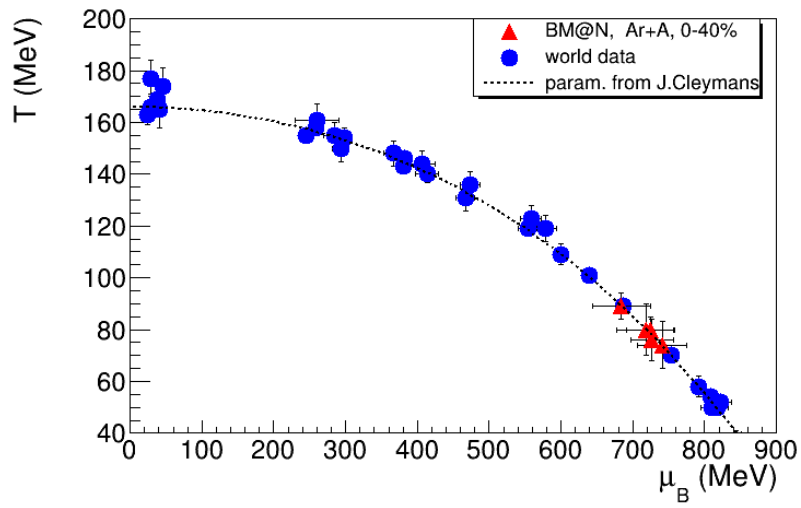[12] J. Cleymans, H. Oeschler, K. Redlich, and S. Wheaton, Phys. Rev. C 73, 034905 (2006).

Figure 9: Freeze-out (T, μ_B) parameters for A+A collisions. BM@N results are from this study, world data and the parameterization for the freezeout line (dashed line) are from [12]

.